Available online at www.sciencedirect.com
SCIENCE DIRECT
Journal of Applied Geophysics 60 (2006) 27–40
JOURNAL OF APPLIED GEOPHYSICS
www.elsevier.com/locate/jappgeo

An experimental study of organic pollutant effects on time domain induced polarization measurements

E. Martinho [a,*], F. Almeida [b], M.J. Senos Matias [b]

[a] Department of Mining Engineering, Technical University of Lisbon, 1049-001 Lisbon, Portugal
[b] Department of Geosciences, University of Aveiro, 3810-193 Aveiro, Portugal

Received 2 November 2004; accepted 22 November 2005

Abstract

Laboratory results from the application of the time domain induced polarization method to the study of organic contamination in soil samples are presented. IP effects for uncontaminated and contaminated (gasoline, isopentane, toluene and benzene) clayey soil samples were measured in the laboratory.

The data were processed to obtain the sample resistivity, resistance, chargeability, capacity, amplitude and decay constant, in order to establish their interdependency, as well as, the behaviour of the main experimental variable involved, that is, the degree of contamination. The results show that minimum values for the chargeability, decay constant and capacity, are reached for a certain amount of pollutant, and a contamination model is proposed using the equivalent circuit theory applied to IP phenomenon.

Thus, a process whereby organic molecules coat clay particle surfaces is proposed and a decrease in the expected membrane polarization effect can explain the interaction between clay minerals and organic molecules.

Finally, the capacity allows a better separation between contaminated and uncontaminated areas than that provided by chargeability and decay constant, as it defines a threshold, which does not depend on the pollutant concentration.

Keywords: Contamination; Hydrocarbons; Resistivity; Induced polarization

1. Introduction

Oil products constitute one of the main types of organic contaminants in the soil. In order to understand the effects caused by oil contamination the polarization mechanisms in soil/organic mixtures must be understood.

Several environmental studies have used geophysical methods to delineate oil-contaminated sites (Benson et al., 1991, 1997; Sauck et al., 1998; Sauck, 2000; Atekwana et al., 2000). These studies show that hydrocarbon plumes may be delineated either as areas of high resistivity (Benson, 1991; Benson et al., 1997), since hydrocarbons typically have higher resistivity than interstitial water (Asquith and Gibson, 1982), or as low resistivity zones (Benson et al., 1991; Benson, 1992; Sauck et al., 1998; Atekwana et al., 2000) due to biodegradation of hydrocarbons that tends to increase the amount of total dissolved solids (TDS) in the interstitial water.

The induced polarization method has been recognised as a useful method in the detection of organic liquids electrical response both in field (Vanhala et al., 1992; Binley et al., 1998) and laboratory conditions (Vanhala and Soininen, 1995; Vanhala, 1997; Klitzsch et al., 1998).

* Corresponding author. Fax: +351 218417111.
E-mail address: emar@mail.ist.utl.pt (E. Martinho).

0926-9851/$ - see front matter © 2005 Elsevier B.V. All rights reserved.
doi:10.1016/j.jappgeo.2005.11.003

In particular, the spectral induced polarization (SIP) method has been used in contamination studies by organic chemical liquids (Vanhala et al., 1992; Vanhala and Soininen, 1995; Vanhala, 1997). Given the equivalence between time and frequency domains herein it is proposed to carry out laboratory investigations in the time domain.

Laboratory investigations were carried out over clayey soil samples, of different grain size compositions and contaminated with several organic chemicals.

At first, IP effects were analysed in gasoline contaminated soil samples. The processed data were analysed in order to establish the interdependency among the electrical parameters, as well as, the behaviour of the different experimental variables involved, that is, time of impregnation, grain size and contamination degree. The results show similar behaviour for the analysed electrical parameters from two different grain size compositions (fraction < 2 mm and fraction < 1 mm).

Then, several gasoline components (isopentane, toluene and benzene) were used as contaminants in order to investigate their IP response. Finally, from the laboratory results, a contamination model is proposed and equivalent circuit theory is applied to the induced polarization effect.

2. IP time domain-basic concepts, laboratory system and data processing

2.1. Basic concepts

The induced polarization method is based on the nearly direct current, electrical resistivity rock behaviour. Rock resistivity can be measured in field or laboratory conditions and, in this study, resistivity and induced polarization measurements were carried out in laboratory by using cylindrical samples and applying four electrode configurations.

Often, a material electrical resistance is expressed in terms of its resistivity. If the resistance between opposite faces of a conducting body of length l and uniform cross section area S is R, the resistivity, ρ, is expressed as

$$\rho = \frac{RS}{l}(\text{ohm}\cdot\text{m}). \tag{1}$$

And its conductivity σ $(=1/\rho)$ is defined as the reciprocal of the resistivity and is measured in Siemens per meter (S/m).

The electric conduction in most rocks is essentially electrolytic as most mineral grains (except metallic ores and clay minerals) are insulators and, therefore, electric conduction is done through the interstitial water in pores and fissures. The resistivity of porous sedimentary formations is variable and dependant on the degree of saturation and nature of pore electrolytes. The electrical resistance, R, of a prismatic rock sample, Fig. 1, length l and cross section S is (Orellana, 1982):

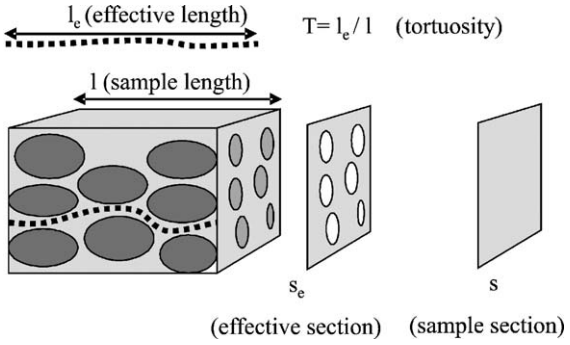

Fig. 1. Prismatic rock sample, showing the matrix and the irregular network of tube conductors. l Sample length; l_e tube conductors length, effective length (Tortuosity is defined as the ratio between l_e and l).

$$R = \rho_r \frac{l}{S}. \tag{2}$$

And ρ_r is the rock sample resistivity. As conduction is done mainly through electrolyte filled pores, with a resistivity ρ_w, then

$$R = \rho_w \frac{l_e}{S_e}. \tag{3}$$

Where l_e is the mean effective length of the tube conductors and S_e is their effective section. Hence S_e corresponds to the effective section from the conduction point of view. Thus from (1) and (2):

$$\rho_r = \rho_w \left(\frac{l_e}{l}\right)\left(\frac{S}{S_e}\right) \tag{4}$$

And multiplying and dividing (4) by l and l_e, respectively:

$$\rho_r = \rho_w \left(\frac{l_e}{l}\right)^2 \left(\frac{Sl}{S_e l_e}\right). \tag{5}$$

The ratio between the mean effective length of the conductive tubes and the sample length is the so called tortuosity, T, that is:

$$T = \frac{l_e}{l}. \tag{6}$$

The rock sample volume is Sl and the volume corresponding to the pores is $S_e l_e$, thus rock porosity ϕ can be written as

$$\phi = \frac{S_e l_e}{Sl}. \tag{7}$$

And from Eqs. (5), (6) and (7)

$$\phi = \frac{V_e}{V_r}. \tag{8}$$

Where V_e is the overall pores volume ($S_e l_e$) and V_r is the rock volume (Sl), that is, porosity has no dimensions and can be written as a percentage of the total rock volume. Rock resistivity can be written as

$$\rho_r = \left(\frac{T^2}{\phi}\right)\rho_w = F\rho_w. \tag{9}$$

Where

$$F = \frac{T^2}{\phi} \tag{10}$$

And F is the so called formation coefficient that depends both on tortuosity, T, and porosity, ϕ.

From Eqs. (9) and (10) it is clear that the organic chemicals presence, as well as other pollutants in general, in the soil will affect the parameters in Eqs. (9) and (10), hence they will be used later in this work, in order to justify and discuss contamination models.

IP principles and methods have been thoroughly described in the literature (Sumi, 1961, Hallof, 1967; Bertin and Loeb, 1974; Bertin and Loeb, 1976; Sumner, 1976; Song and Vozoff, 1985; Apparao, 1997). In broad terms IP data can be obtained by sampling the time decaying potentials observed after switching off DC currents or by measuring the electrical response to the use of currents with different frequencies. Thus, it is possible to conduct time and frequency domain measurements, respectively.

When an electric current is switched off the potential does not decay to zero instantaneously, Fig. 2. The primary potential (V_p) drops immediately to a certain value (V_s) and then starts decaying monotonously to zero, in accordance with a function $f(t)$. On the other hand, when the current is switched on the potential difference does not reach a maximum value immediately, but it will show a slight increase until it stabilizes at its maximum.

Thus, an IP decay curve represents a time varying potential originated by internal currents, in the vicinity of polarizable media. These currents originate from electrical charges reaching equilibrium after an external field is removed.

Basically, IP is a current effect caused by several electrochemical mechanisms such as ion diffusion near

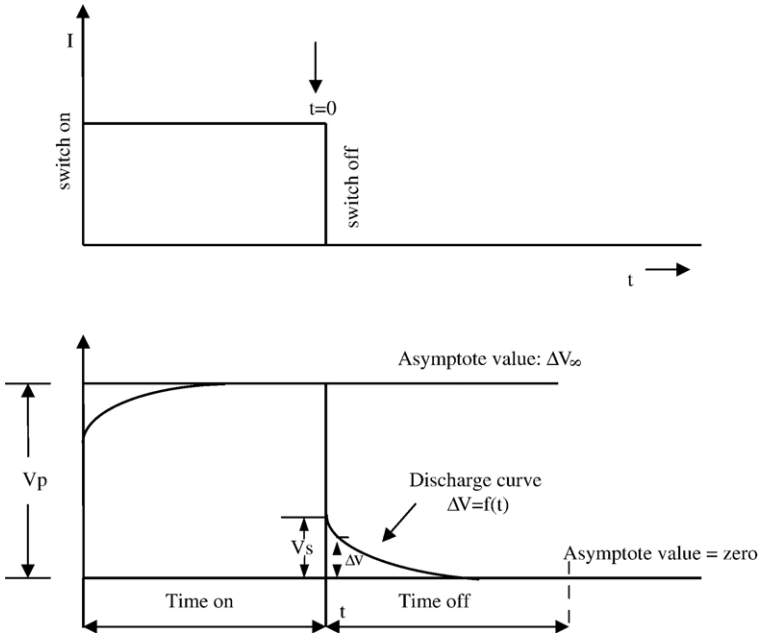

Fig. 2. IP time domain phenomenon: current pulse and resulting voltage. Primary potential (V_p) decays to a secondary potential (V_s) and then follows a monotonous decay with time $-f(t)$.

metallic minerals and, to a less extend, near no metallic minerals, redox reactions between electrolytes and minerals and ion mobility within the electrolyte that fills rock pores.

The IP phenomenon can be modelled with equivalent parallel circuits composed by two resistances (R_{dc} and R_b) and one capacitor (C), such as the one in Fig. 3. In this case, R_{dc} represents the behaviour of resistive ionic conduction in unmineralized current paths near a metallic mineral. The resistor R_b represents the resistance due to blocked conduction paths within mineralised rock, and the capacitor C can be associated with the double-layer capacitance and Warburg impedance (Sumner, 1976).

IP decay curves (Fig. 2) are a very important representation of the effect and several functions have been proposed to describe them. According to the equivalent circuit (Fig. 3) decaying can be described by an exponential function, Sumner (1976). Other authors, such as Wait (1958), Scott and West (1969), have suggested a logarithmic dependence. In this case, at the beginning of the curves potential drops instantaneously from V_p to V_s and a logarithmic decay occurs afterwards. Others, Keller (1959) and Bertin e Loeb (1974), proposed that the decay curve can be obtained by the summation of several exponential functions, that is accepting that the curve contains several components, each one with different time constants that could correspond to different effects. More recently, Slatter (2002) and Titov et al. (2004) obtained a power law dependence for IP measurements carried out on clay free unconsolidated sediments from a sandy aquifer and unsaturated sands, respectively.

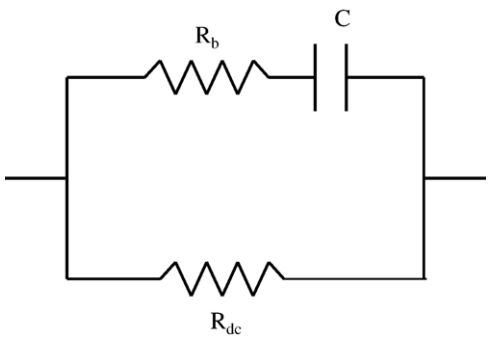

Fig. 3. Equivalent circuit to simulate the IP phenomenon. The circuit is composed by two resistances (R_{dc} and R_b) and one capacitor (C). R_{dc} represents the behaviour of resistive ionic conduction in unmineralized current paths near a metallic mineral. R_b represents the resistance due to blocked conduction paths within mineralised rock. The capacitor C can be associated with the double-layer capacitance and Warburg impedance (After Sumner, 1976).

Therefore, it seems that IP decay curves can be reconstructed using different type functions and it is likely that their shape depends on the nature of mineralization, soils texture and electrolyte composition (Sumner, 1976; Vanhala, 1997).

Bearing in mind the previous discussion, in this work logarithmic functions, $V=a+b\ln(t)$, exponential functions, $V=ae^{bt}$, and power functions, $V=at^b$, were used and tested. However, it was found that the power function describes the experimental curves closer (Martinho, 2003). Data analysis demonstrates that, on one hand, the amplitude (parameter a in $V=at^b$) has the same behaviour as that of the resistivity (Fig. 7(a) and (c)) and, on the other hand, the decay constant behaviour (parameter b in $V=at^b$) is similar to that of the chargeability (Fig. 8(a) and (c)). Hence, amplitude is related with the resistance, thus with the resistivity, whilst the decay constant is related with the chargeability.

Although power functions have been proposed before (Slatter, 2002; Titov et al., 2004), so far there is no appropriate equivalent circuit to describe them. Nevertheless, a simple equivalent circuit, as that on Fig. 3, will still be considered as a good approximation to simulate the IP phenomenon.

As it was mentioned before, IP effects have been approached by different types of equivalent circuits and several decay functions have been proposed. That is, real systems are very complex and it is clear that further research, beyond the scope of this work, has to be done.

The time-domain analysis measures the decaying voltage across R_{dc}, as a result from the discharging of a capacitor through resistances R_b and R_{dc}. The observed transient voltage can be expressed as (Sumner, 1976):

$$V_t = V_p\left[\frac{R_{dc}}{R_{dc}+R_b}\right]e^{\frac{-t}{\tau}}. \tag{11}$$

Where $V_p = IR_{dc}$, and the time constant $\tau=(R_b+R_{dc})C$. The secondary voltage V_s is measured at time $t=0$ and is normalized by the primary voltage V_p, defining the chargeability, M, as the ratio V_s/V_p, that is:

$$M = \frac{V_s}{V_p} = \frac{R_{dc}}{R_{dc}+R_b}. \tag{12}$$

The integrated area under the decay voltage curve normalized by V_p is an indication of the capacitance C value, since the time constant of the decay voltage is given by $(R_{dc}+R_b)C$. The integrated voltage has also been called the chargeability M, that is:

$$M = \frac{1}{V_p}\int_{t_1}^{t_2} V_t dt \tag{13}$$

And from the equivalent circuit (Sumner, 1976)

$$M = R_{dc}C. \quad (14)$$

The integrated signal measurement depends directly on the capacitance C. If C can be used as diagnostic parameter for polarizable rocks, it can be estimated dividing M by R_{dc}.

2.2. Laboratory system

The developed laboratory measurement system is a GPIB (General Propose Interface Bus) controlled system (Martinho and Almeida, 1998) that can carry out electrical measurements. This system (Fig. 4) is able to obtain measurements with a trace length of 50 s at a rate of ten samples per second (with a sample interval of 0.1 s that records frequencies lower than 5 Hz). This laboratory system includes a current source, a digital voltmeter, a BUS IEEE-488 interface and a computer.

In order to carry out laboratory measurements a PVC cylindrical tube, with a 3.75 cm diameter, was used as a sample hold. Specially designed ceramic porous electrodes and non-polarizable 3 cm long Ag/AgCl electrodes were used as current and potential electrodes, respectively.

The measurements were done immediately after the sample was prepared, lasted 30 min, and a 0.0001 mA current with a 4 s pulse (relaxation time) was used.

Several tests were done to evaluate and optimize the system (Martinho, 2003). These tests involved the data acquisition system as well as the investigation of the influence of some parameters, such as, array geometry, current intensity, potential electrode characteristics, sample holder and connectors. The electrolyte influence on the IP measurements was also checked (Martinho, 2003).

2.3. Data processing and IP curves inversion

The data were processed to obtain the sample resistivity, resistance R_{dc} and R_b, chargeability, capacity, amplitude and decay constant. Chargeability was computed from the area below the decay curve normalized with respect to primary voltage. In some cases, when chargeability departed from a defined tendency, this parameter was also calculated from the fifth and tenth sampling steps, that is V_s/V_p for $t=0.5$ s and V_s/V_p for $t=1$ s. For both procedures, chargeability values were computed as the arithmetic mean of six chargeability values obtained from six decay curves in each data file.

The resistance R_{dc}, capacity C, resistance R_b values were computed using the equations previously described. Capacity, C, computation used chargeability values determined from the area below the decay curves. The amplitude and decay constant parameters were also computed by fitting a function $V=at^b$ to the IP curves.

A theoretical model (Fig. 5(c)) was obtained by the summation of translated Heaviside outputs (Fig. 5(b)) that are obtained by convolution of the Heaviside step system output with the translated Dirac distributions (Fig. 5(a)) (Almeida, 1993).

The fit between the computed and the laboratory data, obtained by minimization of quadratic differences summation between model and laboratory data, is

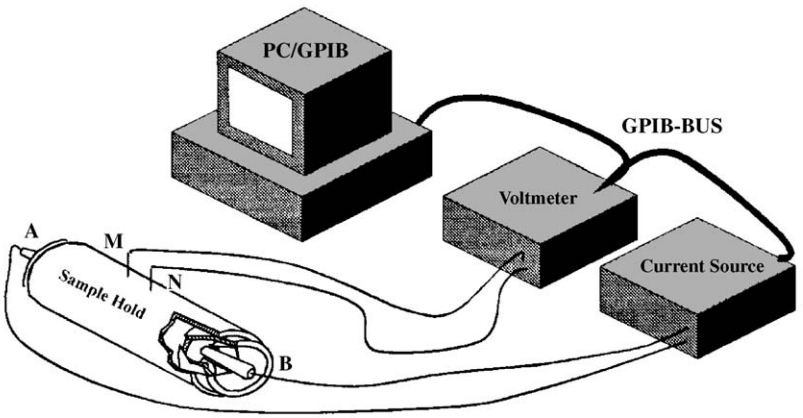

Fig. 4. Laboratory measurement system: current source, digital voltmeter, BUS IEEE-488 interface and computer. The sample hold is a PVC cylindrical tube where the porous ceramic and non-polarizable Ag/AgCl electrodes, used as current and potential electrodes, respectively, are incorporated.

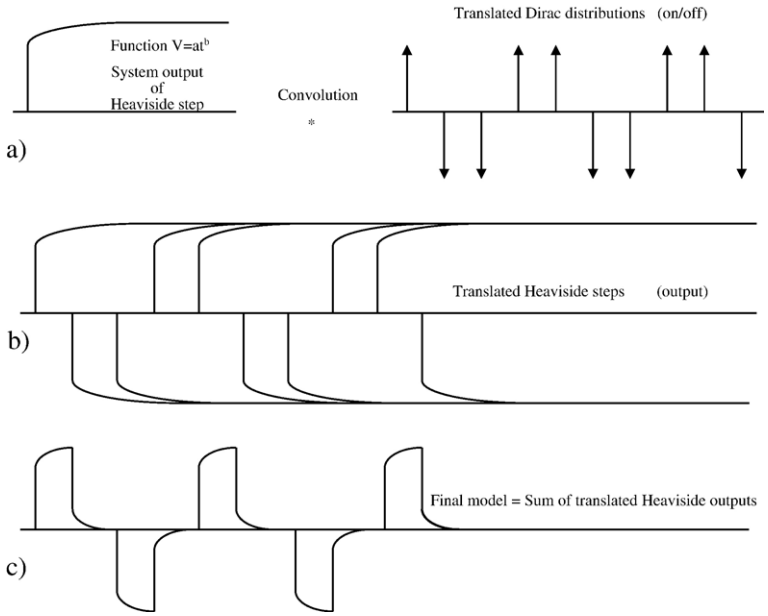

Fig. 5. Theoretical model, (c), obtained by the summation of translated Heaviside outputs, (b), are obtained by the convolution of the Heaviside step system output with the translated Dirac distributions, (a).

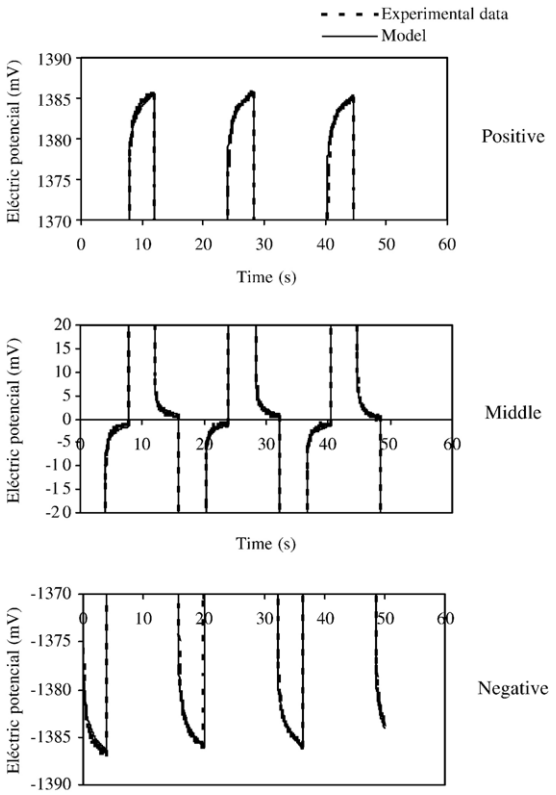

Fig. 6. Fit between the experimental and model decay data as obtained by the minimization of the quadratic differences summation between model and laboratory data.

shown in Fig. 6. In order to obtain a better fit the first and the last two points of the decay curves were not used. In accordance with Sumi (1961), the first decay curve points can be affected by electromagnetic induction effects originated when switching off the electrical current, whilst the last points can show electrical polarization produced by different electrolyte concentrations caused by the current in the current electrodes or in the diffuse layer. Therefore, to avoid these problems the first two samples (0.1 and 0.2 s) were rejected.

3. Soil and water sample

Laboratory studies were done using soil samples obtained in the Aveiro University Campus. The soil was dried in a ventilated stove at a temperature of 40 °C and separation was done into two classes, one with a grain size smaller than 2 mm and another with grain size smaller than 1 mm. Table 1 shows the soil

Table 1
Grain-sizes analysis results of the soil sample for the fraction <1 mm

Grain-size analysis (g/kg)				Texture
Coarse sand $0.2<\varnothing<2$ mm	Fine sand $0.02<\varnothing<0.2$ mm	Silt $0.002<\varnothing<0.02$ mm	Clay $\varnothing<0.002$ mm	
430	349	84	137	Sandy loam

Table 2
Physical and chemical properties of the soil sample (fraction <1 mm)

Parameters		Result
pH (H_2O)		7.2
Organic carbon (g/kg)		2.9
Organic mater (g/kg)		5.0
CEC (cmolc/kg)		4.14
Cation exchange (cmolc/kg)	Ca	4.65
	Mg	0.50
	K	0.14
	Na	0.07
	Mn	Not detectable
Base saturation (%)		Saturated

Base saturation = $S \times 100 / T$.
S—sum of the exchange bases; T—total cation exchange capacity.

samples grain size analysis in accordance with the Atterberg scale.

The mineral composition of the coarse fraction was studied optically, and the finest fraction (<2 μm) was studied by X-ray diffraction. The main minerals in both coarse and fine fractions were quartz, feldspar, micas (biotite and muscovite) and kaolinite. The physical and chemical properties of the soil are given in Table 2.

Thus, physical, chemical and mineralogy analysis shows that: 1) soils have a sandy loam texture due to a small clay fraction (<14%); 2) soils are neutral, (pH value = 7.2); 3) in the small clay fraction, the predominant clay mineral (kaolinite) and the low contents of organic mater (5 g/kg), give a low cation exchange capacity (4.14 $cmol_c$/kg) to this soil; 4) is base saturated and 5) Ca is the dominant exchange cation.

The characteristics of the water used in this study are given in Table 3.

4. Gasoline contaminated samples

4.1. Samples preparation

The first stage of sample preparation was the calculation of the PVC tube capacity (220 cm^3) and the volume of water necessary to saturate de soil samples (70 cm^3 for the fraction <2 mm and 100 cm^3 for the fraction <1 mm).

Uncontaminated samples (fraction <2 mm and fraction <1 mm) were prepared by using water as the electrolyte, and gasoline contaminated samples were impregnated with increasing rates of water versus gasoline (fraction <2 mm, gasoline + water = 70 cm^3; and fraction <1 mm, gasoline + water = 100 cm^3).

At first, each sample was prepared by mixing soil and gasoline and then water was added. Different concentrations of gasoline were used for each grain size (7%, 14% and 21% for fraction <2 mm and 5%, 10%, 20%, 30% and 40% for fraction <1 mm). The largest percentage of gasoline used in fraction <2 mm was 21%, because for larger quantities the data were very noise and therefore meaningless.

The water and the pollutant partial porosity for each grain size are given in Table 4 (the water and pollutant partial porosity were calculate dividing the water and pollutant volume by the soil sample volume).

4.2. Results

Figs. 7 and 8 show the results obtained for each experiment. Thus Figs. 7(b), (d), 8(b) and (d) show the evolution with time for each parameter, for the two samples and different gasoline / water ratios; on the other hand, Figs. 7(a), (c), 8(a) and (c) show the time average data behaviour for increasing gasoline / water ratios.

As it can be seen, resistivity and amplitude (resistance) are directly related with time (Fig. 7(b), (d)). Even though these parameters are higher for the fraction <2 mm, their behaviour is constant for the two grain sizes, that is, a slow decrease with time and an increase with gasoline concentration.

Fig. 8(b) and (d) show a noisy variation of chargeability and decay constant with time. However, the average values (Fig. 8(a) and (c)) are more interesting. The fraction <1 mm shows high chargeability in absence of the pollutant, which can be explained by the high clay quantity. The decay constant parameter shows always higher values for the coarse fraction.

In general, the two parameters have similar behaviour with respect to gasoline concentration, that is, they decrease with increasing gasoline concentration and are relatively constant for the concentration interval 10–20%. Then they increase until pollutant sample saturation is reached. The mean chargeability and

Table 3
Water analysis

pH	Temperature (°C)	Conductivity (Ω m)	HCO_3^-	Cl^-	NO_3^-	SO_4^{2-}	Na^+	K^+	Ca^{2+}	Mg^{2+}
			mg/l							
7.3	15.4	29.9	102	29	1	43	58	7	7	7

Table 4
The water and pollutant partial porosity for each grain size

Soil sample volume=220 cm^3							
f<2 mm				f<1 mm			
Pollutant (cm^3)	Water (cm^3)	Water partial porosity (ϕ)	Increment porosity ($\Delta\phi$)	Pollutant (cm^3)	Water (cm^3)	Water partial porosity (ϕ)	Increment porosity ($\Delta\phi$)
0	70	0.32	0	0	100	0.45	0
5	65	0.30	0.02	5	95	0.43	0.02
10	60	0.27	0.05	10	90	0.41	0.04
15	55	0.25	0.07	20	80	0.36	0.09
				30	70	0.32	0.13
				40	60	0.27	0.18

decay constant is less grain size dependant and the minimum threshold reached can be regarded as an indicator of the pollutant presence (gasoline).

It must be pointed out that for very high gasoline concentrations the curves invert their tendency and start rising again. This is similar to the cases of very low gasoline concentration and, hence, the results can be difficult to interpret. However, cases where such high pollutant concentrations occur should be rare in field situations and, if they do occur, they should be restricted to an area in the close vicinity of a spill.

5. Gasoline components contaminated samples

Further laboratory measurements were carried out in order to study the dependency of the chargeability and decay constant parameters with some of the most common gasoline components.

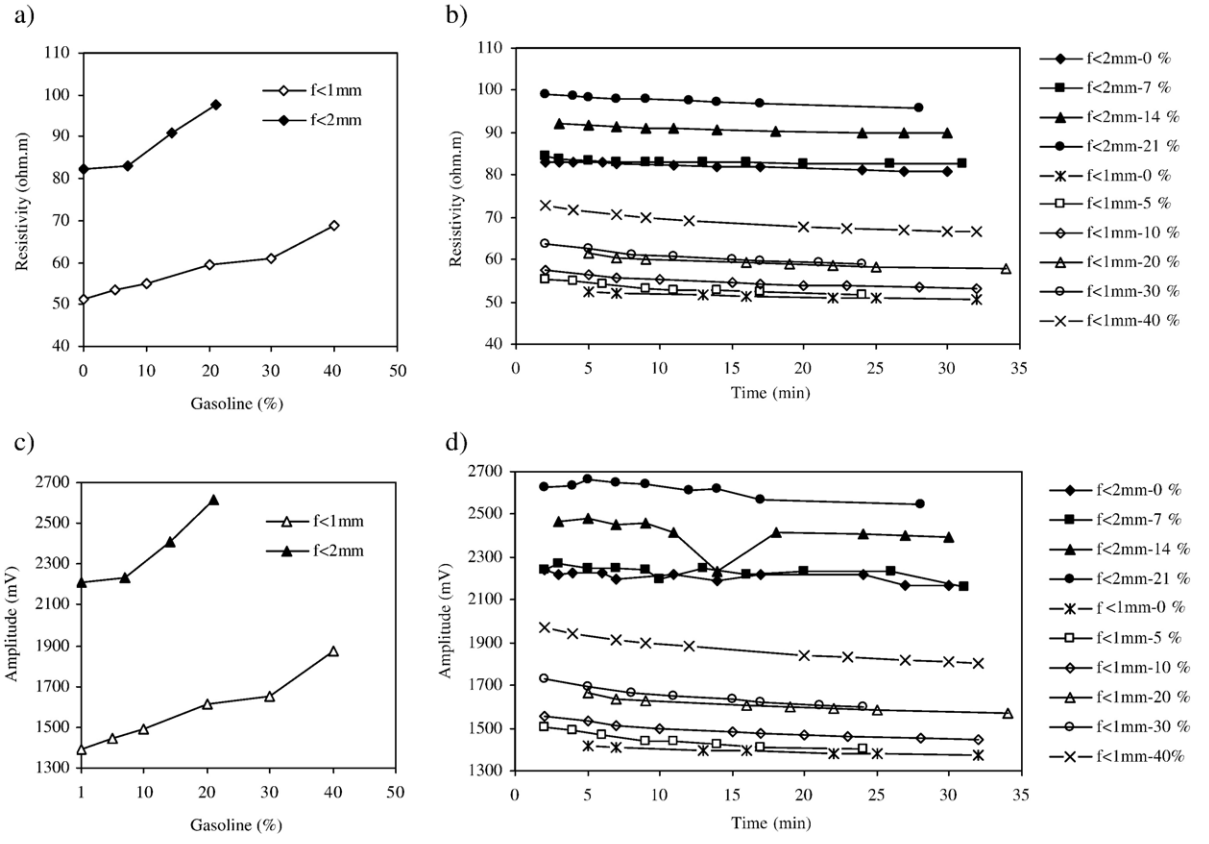

Fig. 7. Experimental results: (b) and (d) time dependant data; (a) and (c) time average values versus percentual gasoline/water ratio. (a) and (b) resistivity data; (c) and (d) adjusted amplitude function.

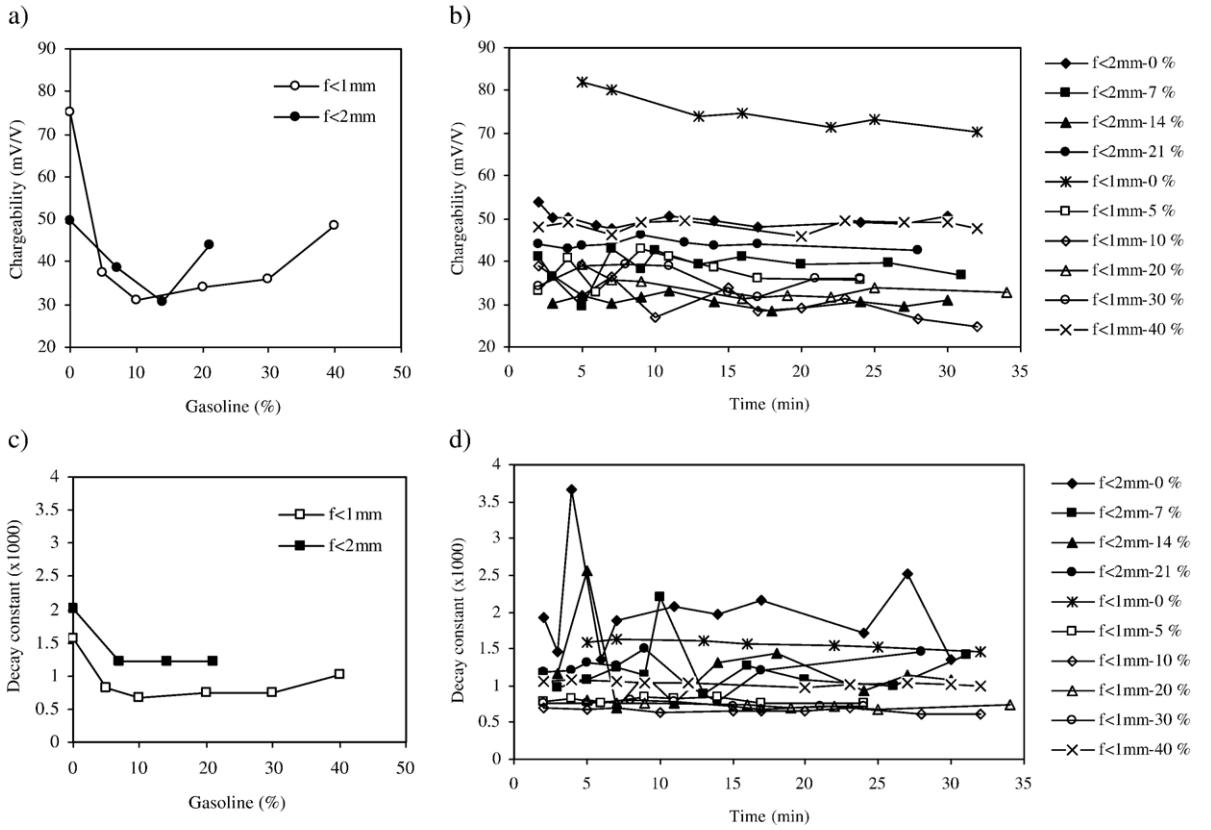

Fig. 8. Experimental results: (b) and (d) time dependant data; (a) and (c) time average values versus percentual gasoline/water ratio. (a) and (b) chargeability data; (c) and (d) adjusted decay constant function.

The used gasoline components were isopentane, toluene and benzene. Sample preparation was done as before but only the grain size samples < 1 mm were used so that higher pollutant concentrations could be studied.

5.1. Results

Fig. 9 compares the time average values behaviour for each parameter (resistivity, chargeability and decay constant) with increasing pollutant/water ratios for all the pollutants. Amplitude data are not discussed as its behaviour is similar to that of the resistivity as shown for gasoline (Fig. 7).

Fig. 10 depicts the chargeability for toluene as computed for $t=0.5$ s and $t=1$ s. As it can be seen, the behaviour is very close to the one shown for the chargeability in Fig. 9(b). The same conclusion can be drawn for all the other pollutants (Martinho, 2003).

All parameters show similar behaviour for the different contaminants. Thus, resistivity increase with increasing contaminant concentration (Fig. 9(a)), chargeability and decay constant decrease with increasing pollutant concentration (Fig. 9(b) and (c)). A fairly constant level is observed for a pollutant concentration interval of 10–20%, and afterwards the values increase until pollutants reaches sample saturation (Fig. 9(b) and (c)).

Each parameter time evolution is smooth and a decrease of resistivity is observed as for the gasoline case. However, for higher concentrations, the resistivity decrease is more pronounced, as it should be expected from Eq. (9).

In accordance with this equation porosity, tortuosity and electrolyte resistivity variations will vary rock resistivity. Thus, porosity can change either if there is not a thorough sample homogenisation or by electrolyte diffusion. On the other hand, more complete homogenisation and porosity increase with time favour shorter circuit paths, that is, a decrease in tortuosity. Tortuosity changes can also occur by pollutant agglomeration because of pollutant immiscibility with the electrolyte.

Finally, reactions between the pollutant and the electrolyte will vary the resistivity of the later one. However it is difficult to accept this hypothesis as

experimental data show that curves behaviour is similar for all pollutants.

Therefore, the curve parameters behaviour can be associated with the homogenisation process, a pollutant agglomeration phenomenon or a chemical process concerning the increase of the ions number in the electrolyte. That is, the interaction between the minerals and the organic molecules can alter the redox potential,

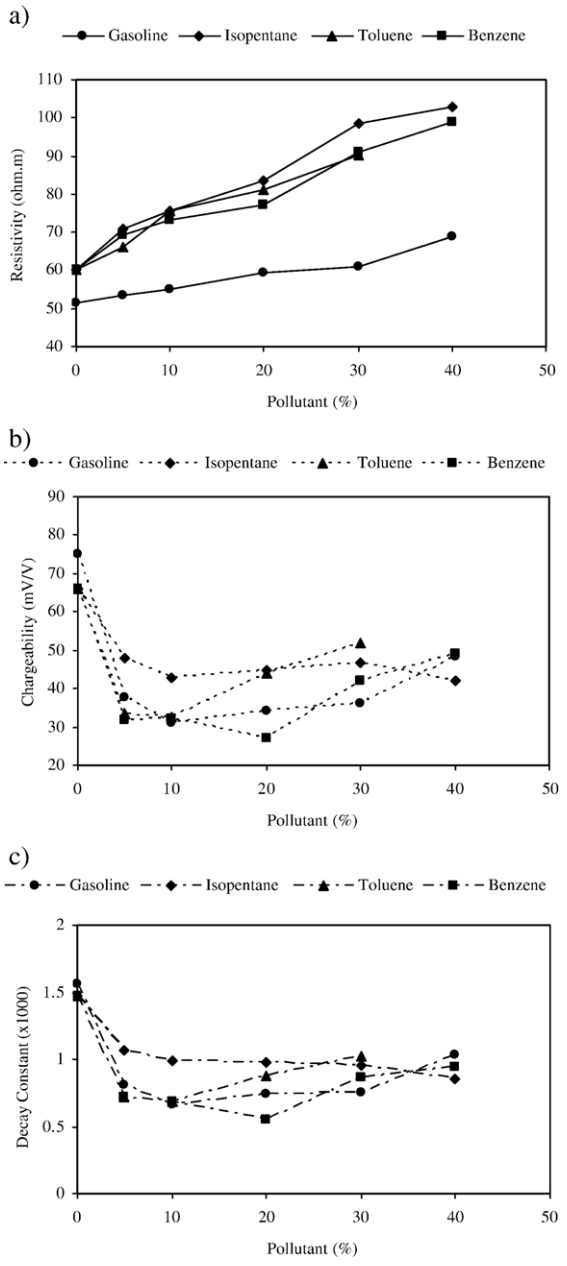

Fig. 9. Experimental results. Time average values versus pollutant/water ratio. (a) Resistivity data; (b) chargeability data; (c) decay constant data.

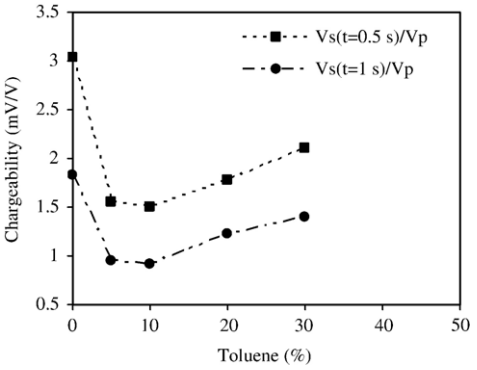

Fig. 10. Toluene computed chargeability for the fifth and the tenth sampling steps.

increasing the dissolved forms of ions (as Fe ions) in aqueous solution (Kölling, 1986).

The chargeability and decay constant do not show any peculiar trend with time, as for gasoline, apart from decreasing when pollutant concentration increases. The overall curves for the pollutants (Fig. 9) show that resistivity is lower for gasoline and higher for its components (Fig. 9(a)). The slope of adjusted curves for the resistivity is also lower for the gasoline (Fig. 9(a)).

Chargeability and decay constant minimum values vary with pollutant, as shown in Fig. 9(b) and (c), but the general behaviour is similar. Benzene gives the lowest value, while isopentane gives the highest value. Isopentane, an aliphatic hydrocarbon, seems to have less influence in the polarization effect and, thus, its interaction with clay minerals is not as intense as that for gasoline, toluene and benzene. Benzene gives lower resistivity values and is more influent in the polarization effect. This must be related to the fact that benzene, toluene and gasoline are aromatic hydrocarbons and are organic chemicals that can interact with clay minerals (Gomes, 1986).

6. Contamination model

The mechanisms that cause the polarization effect in soil/organic mixtures are not well known, but can be related with the interaction between clay minerals and organic molecules.

In general, rocks consist of minerals (matrix) and pores which form an irregular and tortuous net filled with electrolyte and, theoretically, several interaction ways are possible. It is now proposed to investigate a model that can justify the IP effects produced by organic pollutants in soils.

Since the resistivity, ρ_r, can be defined by Eq. (9) and the addition of organic chemicals changes both the

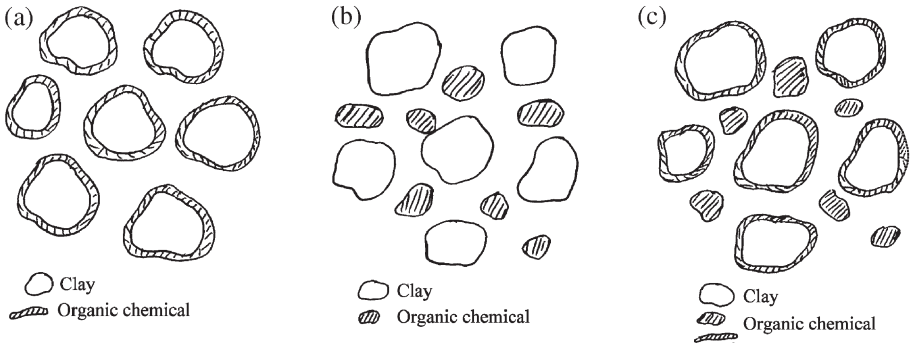

Fig. 11. Possible contamination models: (a) porosity variation as a result of clay particles coating by organic molecules; (b) porosity and tortuosity variation, when clay particles are not coated by organic molecules, but these molecules occupy pores just like a mineral grain and (c) porosity and tortuosity variation caused by both models (a) and (b).

tortuosity and porosity, three different models can be considered (Fig. 11): model (a) porosity change due organic molecules that coat the surfaces of clay particles; model (b) porosity and tortuosity change when organic molecules that do not coat clay particles surface but occupy the pore-space as a mineral grain; model (c) change porosity and tortuosity according to the combination of models (a) and (b).

Olhoeft (1985) explained the low-frequency effect by a process whereby organic molecules coat the surfaces of clay particles, inhibiting the cation-exchange process. Therefore, as work hypothesis, only model (a) will be discussed here in.

Thus, if Eq. (9) is differentiated

$$\mathrm{d}\rho_\mathrm{r} = \frac{\partial \rho_\mathrm{r}}{\partial T}\mathrm{d}T + \frac{\partial \rho_\mathrm{r}}{\partial \phi}\mathrm{d}\phi. \tag{15}$$

For model (a), rock resistivity does not change with tortuosity and the partial derivative $\partial\rho_\mathrm{r}/\partial T$ must be zero, that is:

$$\frac{\partial \rho_\mathrm{r}}{\partial T}\mathrm{d}T = 0 \tag{16}$$

And

$$\frac{\mathrm{d}\rho_r}{\mathrm{d}\phi} = \frac{\partial \rho_\mathrm{r}}{\partial \phi} \tag{17}$$

If Eq. (9) is differentiated with respected to phi,

$$\frac{\partial \rho_\mathrm{r}}{\partial \phi} = -\frac{T^2\rho_\mathrm{w}}{\phi^2} \tag{18}$$

And using Eqs. (9) and (18)

$$\frac{\partial \rho_\mathrm{r}}{\partial \phi} = -\frac{\rho_\mathrm{r}}{\phi} \tag{19}$$

From (17) and (19) the derivative of the rock resistivity in order to the porosity can also be computed from the ratio between rock resistivity and porosity values, that is

$$\frac{\mathrm{d}\rho_\mathrm{r}}{\mathrm{d}\phi} = -\frac{\rho_\mathrm{r}}{\phi}. \tag{20}$$

In a sample impregnated with 100 ml of liquid (water+pollutant) when the pollutant amount is increased the effective porosity decreases as pores are occupied by an electrolyte (Table 4). This table shows the variation of the sample effective porosity with the pollutant concentration and, as it can be seen, for the fraction <1 mm, ϕ (water partial porosity) varies from 0,45, when no pollutant is present, to 0.27 for a pollutant volume of 40 cm^3. Hence it is possible to compute the porosity increment ($\Delta\phi$) between each experiment and relate it with the measured rock resistivity, that is:

$$\frac{\mathrm{d}\rho_\mathrm{r}}{\mathrm{d}\phi} = -\frac{\rho_{\mathrm{r}_1}}{\phi_1}, -\frac{\rho_{\mathrm{r}_2}}{\phi_2}, -\frac{\rho_{\mathrm{r}_3}}{\phi_3}, \ldots \tag{21}$$

And

$$\frac{\mathrm{d}\rho_r}{\mathrm{d}\phi} \approx \frac{\Delta\rho_\mathrm{r}}{\Delta\phi} = -\frac{\rho_{\mathrm{r}_i}}{\phi_i} \tag{22}$$

That is, if (22) can be experimentally tested model (a) is acceptable.

The experimental work provided the estimation of the right member of Eq. (22) (Table 5) by using the water partial porosity values for each pollutant concentration value (Table 4), and the last measured resistivity value in each sample. This value was used because it is the one for which the system is more

Table 5
Results of $-\rho_r/\phi$ for pollutants

	Gasoline		Isopentane		Toluene		Benzene	
Pollutant (%)	ρ_r (Ω m)	$-\rho_r/\phi$	ρ_r (Ω m)	$-\rho_r/\phi$	ρ_r (Ω m)	$-\rho_r/\phi$	ρ_r (Ω m)	$-\rho_r/\phi$
0	50.7	–112	59.8	– 132	59.8	– 132	59.8	– 132
5	51.7	–120	70.0	– 162	65.4	– 151	68.5	– 159
10	53.3	–130	75.0	– 183	75.0	– 183	72.3	– 177
20	57.8	–159	82.0	– 226	80.8	– 222	74.7	– 205
30	58.8	–185	96.0	– 302	89.1	– 280	89.4	– 281
40	66.6	–244	100.0	– 367			96.7	– 355

stable (Table 5). The relationship between ρ_i and ϕ_i allows the estimation of $\Delta\rho_r/\Delta\phi$ for each pollutant (Fig. 12).

The results show that, with the exception of gasoline, the linear regression coefficients ($\Delta\rho_r/\Delta\phi$) between ρ_i and ϕ in Fig. 12 are approximate to $-\rho_r/\phi$ (Table 5) for amounts of pollutant between 10% and 20% (the shading values in the Table 5), and thus the proposed model (a) seems to hold for these pollutant concentrations. Experimental data also show that the chargeability reaches a minimum for that concentration (Fig. 9(b)). If model (a) is accepted, then it is probable the occurrence of a double layer effect decrease related with the chargeability decrease, which is in agreement with data from others authors (Olhoeft, 1985). For pollutant concentrations outside the 10–20% interval other mechanisms are needed to explain the IP behaviour.

In Fig. 13(a) it is shown the variation of the capacity C with the amount of pollutant present in the sample, as calculated from equation (14). The parameter C allows the integration of both IP and resistivity information. As it can be seen, the capacity, *C* (Fig. 13(a)), is about 50% (0.02) of the value obtained in uncontaminated samples (0.04). The observed increase both in chargeability and in capacity after the minimum value is reached, is more pronounced in chargeability than in capacity. Thus, it is possible to define the contamination by using the

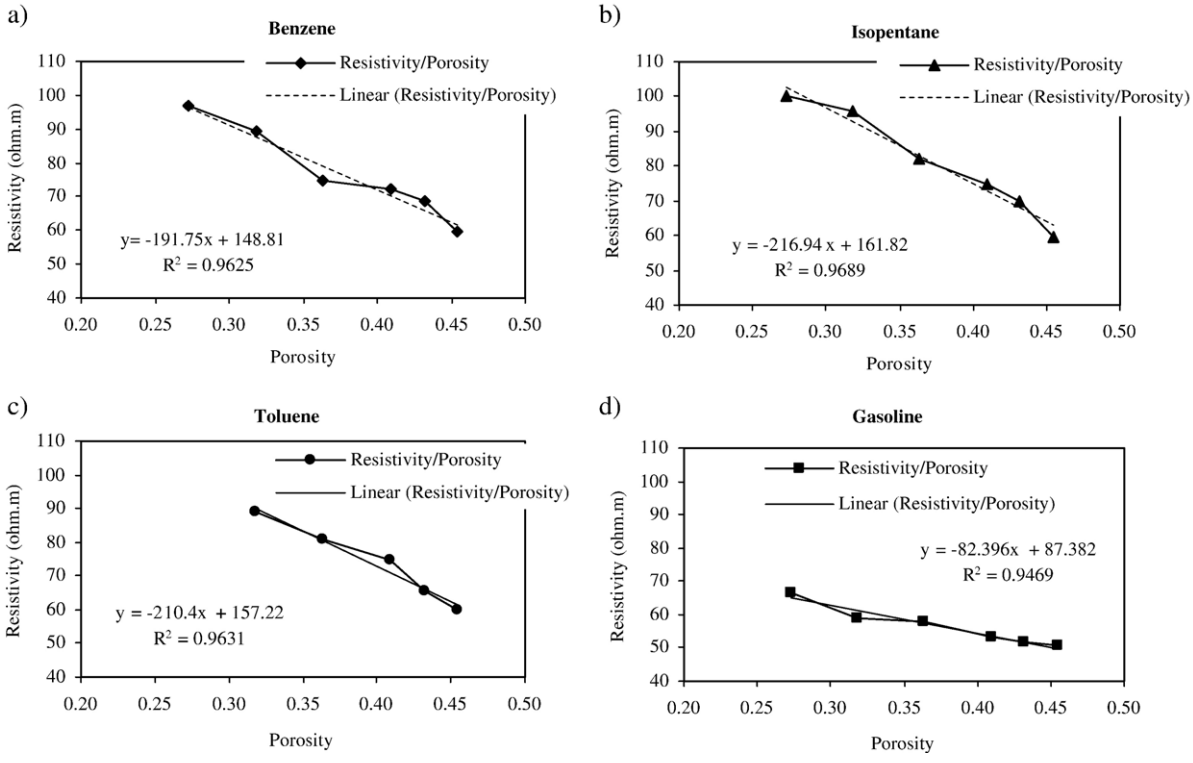

Fig. 12. Linear regression coefficients between ρ_i (Table 5) and P_i (Table 4) for 0%, 5%, 10%, 20%, 30% and 40% of pollutant.

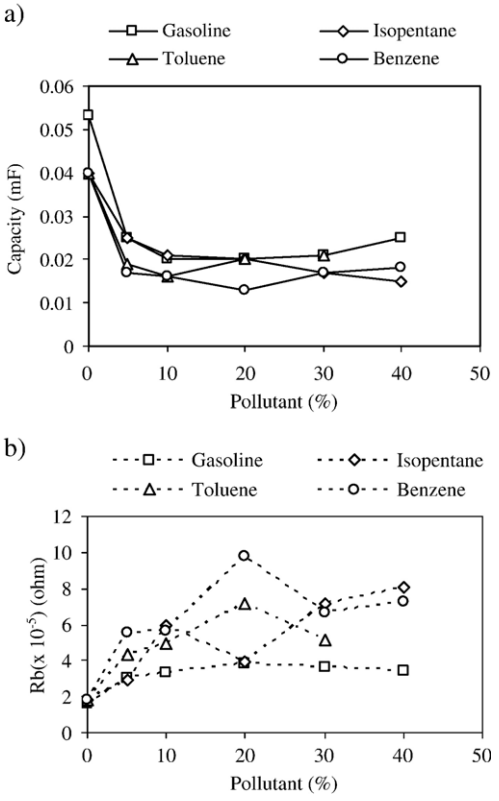

Fig. 13. Mean values of capacity, C (a) and resistance, R_b (b) for different pollutants.

capacity (Fig. 13(a)) which is related with resistance (R_{dc}) and chargeability (Eq. (14)).

As, it is shown in Fig. 13(b), and with the isopentane exception, for pollutant concentrations higher than 20%, the R_b resistance, calculated from Eq. (12) (that is the resistance associated with the capacitor in the electrical circuit of Fig. 3) decreases. This can be interpreted as the reposition of the electrical charges equilibrium is favoured by the decrease in the blocking paths effect by the positive ions.

7. Conclusions

In clayey soils, in particular when minerals belonging to the kaolinite group are dominant, the chargeability decay constant and the capacity behaviour demonstrate that IP time domain measurements can be used in the detection of organic contaminants. Particularly good results have been obtained for pollutant concentrations between 10% and 20%.

Nevertheless it is acknowledged that further studies and experiments are needed for other type of soils, where it is possible that different decay functions may be more appropriate.

With the developed laboratory measurement system it was possible to obtain resistivity and amplitude measurements with a 20% variation between gasoline and isopentane, toluene and benzene. The variation is lower for chargeability (14%) and decay constant (6%).

In spite of stabilization being dependant on physical processes (that is, homogenisation and geometric pollutant redistribution) as well as chemical processes (ion concentration increase on the electrolyte) measurements lasting 30 min demonstrate the stabilization of the system.

The two fractions (<1 and <2 mm) do not show any significant alterations on the IP effect. However it must be pointed out that for the fraction <2 mm, it is shown an increase in the resistivity and in the amplitude parameters as well as an increase in the data noise.

Decay curves can be described through several functions but in this case power functions, $V=at^b$, describe the experimental data closer.

Minimum chargeability, decay constant and capacity values are reached for pollutant concentrations ranging from 10% to 20%. For lower concentrations the soil clay particles should be responsible for the higher recorded values. For higher concentrations more studies should be carried out in order to understand the process.

The interaction between clay minerals and organic molecules can be explained to some extent by a process whereby organic molecules coat clay particles surfaces and, therefore, a decrease in the membrane polarization effect is expected for pollutant concentration in the 10–20% range.

The capacity C allows a better separation between contaminated and uncontaminated samples than that provided by chargeability and decay constant, as it defines a threshold which is not depend on pollutant concentration and, therefore, can be used in future works.

Although there is no sufficient field experience yet, this technique can be used to locate contamination plumes, in conjunction with other geophysical methods. However, more important is its potential use to evaluate and monitor the temporal evolution of contaminated areas previously located by other methods, as pollutant concentration variations are detectable in the experimental model curves herein discussed.

Acknowledgements

The authors wish to thank to Prof. Maria Manuela Abreu for her orientation in sample soil characterization,

Prof. Eduardo Silva for the water analysis and Mrs. Maria João Basto for the X-ray Diffraction.

References

Almeida, F.E.R., 1993. Tripotential Techniques and Orientation Effects in Induced Polarization, unpublished PhD Thesis (in Portuguese), University of Aveiro. 346 pp.

Apparao, A., 1997. Development in Geoelectrical Methods. A. A. Balkema, Rotterdam, Brookfield. 293 pp.

Asquith, G.B., Gibson, C.R., 1982. Basic well log analysis for geologists. American Association of Petroleum Geologists.

Atekwana, E.A., Sauck, W.A., Werkema Jr., D.D., 2000. Investigations of geoelectrical signatures at a hydrocarbon contaminated site. Journal of Applied Geophysics (44), 167–180.

Benson, R.C., 1991. Remote sensing and geophysical methods for evaluation of subsurface conditions. In: Nielsen, D.M. (Ed.), Practical Handbook of Groundwater Monitoring. Lewis Publishers, pp. 143–194.

Benson, R.C., 1992. Integrating seismic, resistivity, and ground penetrating radar to delineate the water table and groundwater contamination. In: Kharaka, Y.K., Maest, A.S. (Eds.), Water–Rock Interaction, Low Temperature Environments, vol. 1. Balkema, pp. 361–365.

Benson, A.K., Frederickson, C., Mustoe, N.B., 1991. Ground penetrating radar, electrical resistivity, soil and water quality studies integrated to determine the source(s) and geometry of hydrocarbon contamination at a site in north-central Arizona. Proccedings 27th Symposium on Engineering Geology and Geotechnical Engineering, pp. 38.1–38.13.

Benson, A.K., Payne, K.L., Stubben, M.A., 1997. Mapping groundwater contamination using dc resistivity and VLF geophysical methods—a case study. Geophysics (62), 80–86.

Bertin, J., Loeb, J., 1974. Traitement "à la main" et sur ordinateur des transistoires en polarization provoquée. Geophysical Prospecting (22), 93–106.

Bertin, J., Loeb, J., 1976. Experimental and Theoretical Aspects of Induced Polarization: 1. Gebrüder Borntraeger, Berlin. 250 pp.

Binley, A., Eriksen, A., Gascoyne, J., Nguyen, T., Kemna, A., 1998. Spectral characteristics at a former industrial site using complex resistivity. Proccedings of the IV Meeting of the Environmental and Engineering Geophysical Society (European Section), Barcelona (Spain), pp. 1–4.

Gomes, C.F., 1986. Clays: What are They and What is Their Use (in Portuguese). Calouste Gulbenkian Fundation, Lisbon. 457 pp.

Hallof, P.G., 1967. An appraisal of the variable frequency IP method after twelve years of application. Symposium on Induced Polarization. University of California, Berkeley. 13 pp.

Keller, G.V., 1959. Analysis of some electrical transient measurements on igneous, sedimentary and metamorphic rocks. In: Wait, J.R. (Ed.), Overvoltage Research and Geophysical Applications. Pergamon Press, London.

Klitzsch, N., Stallmach, F., Jacobs, F., 1998. Laboratory investigation to prove low concentrations of hydrocarbons in soils. Proccedings of the IV Meeting of the Environmental and Engineering Geophysical Society (European Section), Barcelona (Spain), pp. 31–34.

Kölling, M., 1986. Vergleich verschiedener Methoden zur Bestimmung des Redox-Potentials natürlicher Wässer. Meyniana (38), 1–19.

Martinho, E., 2003. Integrated study of Environmental Problems by Geophysical Methods, unpublished PhD Thesis (in Portuguese), Technical University of Lisbon. 269 pp.

Martinho, E., Almeida, F., 1998. Time domain induced polarization experiments on gasoline contaminated samples. Proccedings of the IV Meeting of the Environmental and Engineering Geophysical Society (European Section), Barcelona (Spain), pp. 85–87.

Olhoeft, G.R., 1985. Low-frequency electrical properties. Geophysics (50), 2492–2503.

Orellana, E., 1982. Prospeccion Geoelectrica en Corriente Contínua. Paraninfo, Madrid. 278 pp.

Sauck, W.A., 2000. A model for the resistivity structure of LNAPL plumes and their environs in sandy sediments. Journal of Applied Geophysics (44), 151–165.

Sauck, W.A., Atekwana, E.A., Nash, M.S., 1998. High conductivities associated with an LNAPL plume imaged by integrated geophysical techniques. Journal of Engineering and Environmental Geophysics (2), 203–212.

Scott, W.J., West, C.F., 1969. Induced polarization of synthetic high resistivity rocks containing disseminated sulphides. Geophysics (34), 87–100.

Slatter, L., 2002. Unconsolidated sandy aquifer properties inferred from induced polarization measurements. Denver Annual Meeting, in http://gsa.confex.com/gsa/2002AM/finalprogram/abstract-41645.htm.

Song, L., Vozoff, K., 1985. The complex resistivity spectra of models consisting of two polarizable media of different intrinsic properties. Geophysical Prospecting (33), 1029–1062.

Sumi, F., 1961. The induced polarization method in ore investigation. Geophysical Prospecting (9), 459–477.

Sumner, J.S., 1976. Principles of Induced Polarization for Geophysical Exploration. Elsevier Scientific Publishers, Amsterdam. 277 pp.

Titov, K., Kemna, A., Tarasov, A., Vereecken, H., 2004. Induced polarization of unsaturated sands determined through time domain measurements. Vadose Zone Journal (3), 1160–1168.

Vanhala, H., 1997. Mapping oil-contaminated sand and till with the spectral induced polarization (SIP) method. Geophysical Prospecting (45), 303–326.

Vanhala, H., Soininen, H., 1995. Laboratory technique for measurements of spectral induced polarization response of soil samples. Geophysical Prospecting (43), 655–676.

Vanhala, H., Soininen, H., Kukkonen, I., 1992. Detecting organic chemical contaminants by spectral-induced polarization method in glacial till environment. Geophysics (57), 1014–1017.

Wait, J.R., 1958. Discussions on a theoretical study of induced electrical polarization. Geophysics (23), 144–154.